

Covalent bonding and the nature of band gaps in some half-Heusler compounds

Hem Chandra Kandpal[‡], Claudia Felser[†],
and Ram Seshadri[‡]

[†]Institut für Anorganische Chemie und Analytische Chemie
Johannes Gutenberg-Universität, Staudinger Weg 9, 55099 Mainz
felser@uni-mainz.de

[‡]Materials Department and Materials Research Laboratory
University of California, Santa Barbara CA 93106
seshadri@mrl.ucsb.edu

Abstract.

Half-Heusler compounds XYZ , also called semi-Heusler compounds, crystallize in the $MgAgAs$ structure, in the space group $F\bar{4}3m$. We report a systematic examination of band gaps and the nature (covalent or ionic) of bonding in semiconducting 8- and 18- electron half-Heusler compounds through first-principles density functional calculations. We find the most appropriate description of these compounds from the viewpoint of electronic structures is one of a YZ zinc blende lattice stuffed by the X ion. Simple valence rules are obeyed for bonding in the 8-electron compound. For example, $LiMgN$ can be written $Li^+ + (MgN)^-$, and $(MgN)^-$, which is isoelectronic with $(SiSi)$, forms a zinc blende lattice. The 18-electron compounds can similarly be considered as obeying valence rules. A semiconductor such as $TiCoSb$ can be written $Ti^{4+} + (CoSb)^{4-}$; the latter unit is isoelectronic and isostructural with zinc-blende $GaSb$. For both the 8- and 18-electron compounds, when X is fixed as some electropositive cation, the computed band gap varies approximately as the difference in Pauling electronegativities of Y and Z . What is particularly exciting is that this simple idea of a covalently bonded YZ lattice can also be extended to the very important *magnetic* half-Heusler phases; we describe these as valence compounds *ie.* possessing a band gap at the Fermi energy albeit only in one spin direction. The *local* moment in these magnetic compounds resides on the X site.

PACS numbers: 75.50.-y, 71.20.-b, 75.50.Cc

1. Introduction

The half-Heusler phases XYZ , comprising three interpenetrating *fcc* lattices, constitute an important class of materials with particular regard to their magnetic properties. de Groot[1] and coworkers showed a number of years ago that the half-Heusler compound NiMnSb can be described as a half-metallic ferromagnet, whose computed band structure resembles a metal in one spin direction, and a semiconductor in the other. Since then, and indeed, even prior to that, it has been recognized that the electronic structure and hence properties of Heusler compounds[2] and half-Heusler compounds[3, 4] are very sensitive to the valence electron count.

A number of electronic structural studies have been carried out on the half-Heuslers. We focus here on those studies which systematically address behavior in families of half-Heusler compounds, rather than studies focused on individual ones. From the viewpoint of chemical bonding in these compounds, Whangbo and coworkers[5] have examined the non-magnetic band structures, using the extended Hückel method, of a number of half-Heusler compounds with varying valence electron counts. These authors have recognized that many XYZ half-Heuslers can be thought of as comprising an X^{n+} ion stuffing a zinc blende YZ^{n-} sublattice where the number of valence electrons associated with YZ^{n-} are 18 ($d^{10} + s^2 + p^6$). 18 electron compounds are therefore closed shell species; non-magnetic and semiconducting. They further suggest that the 17 and 19 electron XYZ would undergo a Stoner instability[6] to a ferromagnetic ground state, while the 22 electron compounds (typically with Mn^{3+} at the X site) should be localized moment ferromagnets. The 22 electrons divide themselves into 13 in the majority spin and 9 in the minority spin direction, resulting in a semiconducting gap (half-metallic behavior) in the minority spin direction. Recently, Galanakis *et al.*[7] have placed this “18 electron” rule on a more formal footing.

Pierre *et al.*[3] were amongst the first to recognize the importance of the valence electron count in the half-Heuslers. In more recent work, Tobola and Pierre[4] have emphasized the importance of covalency in these compounds. The Z element is often a pnictogen (As, Sb or Bi) or some other main group element because only covalent bonding would justify the somewhat open half-Heusler structure. Ögüt and Rabe[8] have examined the electronic structures of the compounds $XNiSn$ with $X = Ti, Zr,$ or Hf , and interpreted phase stability and the nature of band gaps. Also important from the approach that we will take here is the work of Wood, Zunger, and de Groot[9] who have examined a number of non-magnetic “stuffed zinc blende” semiconductors, the so-called Nowotny-Juza compounds[10, 11] including half-Heusler phases such as $LiZnP$, in order to control the nature of the band gap (direct or indirect). Nanda and Dasgupta[12] have examined nearly 20 different half-Heusler compounds using the FP-LMTO and LMTO-ASA methods, including a detailed analysis of the bonding and the nature of the band gaps. They argue as we do here, for the very important role played by covalent bonding in these systems. They ascribe half-metallicity to arise in some of the half-Heuslers due to the large $Y-Z$ covalency, in conjunction with large exchange

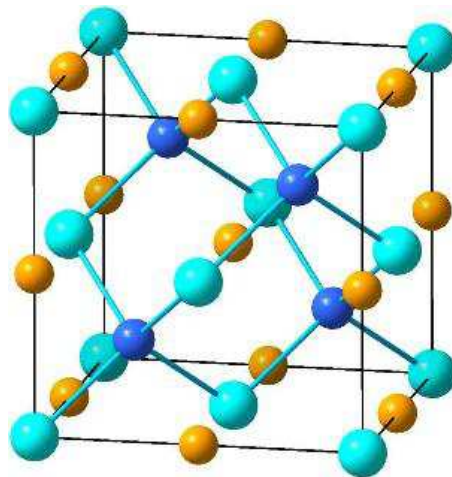


Figure 1. (Color) XYZ Half-Heusler crystal structure in the $F\bar{4}3m$ space group. Cyan Z atoms are at the origin, orange X at $(\frac{1}{2}, \frac{1}{2}, \frac{1}{2})$ and blue Y at $(\frac{1}{4}, \frac{1}{4}, \frac{1}{4})$. Note the tetrahedral zinc blende (diamondoid) sublattice formed by Y and Z .

-splitting due to highly magnetic X ions.

In this contribution, we focus on chemical bonding in 8, 18 and magnetic half-Heusler compounds, and attempt to relate the electronic structure to simple concepts such as the electronegativity of the component species. We also demonstrate covalency and the local nature of the magnetic moment in the magnetic compounds using real-space descriptors derived from first principles theory.

2. Crystal structures and methods

Half-Heusler XYZ compounds crystallize in the space group of zinc blende ($F\bar{4}3m$) with a cubic cell parameter near 6.0 Å. The least and most electronegative elements are X at $(\frac{1}{2}, \frac{1}{2}, \frac{1}{2})$ and Z at $(0, 0, 0)$ forming a rock salt lattice. Y are found at $(\frac{1}{4}, \frac{1}{4}, \frac{1}{4})$ in the centers of tetrahedra formed by Z , as well as by X . Connecting Y and Z reveals the stuffed zinc blende lattice of the half-Heusler structure displayed in Figure 1. There are other, equivalent descriptions of this structure, but this is the one we chose, because it is closest to our description of the chemical bonding.

Density functional theory-based electronic structure calculations were performed using the full-potential Linear Augmented Plane Wave (LAPW) code WIEN2K[13] to optimize cell volumes of the different half-Heusler compounds described here. The electronic structural descriptions made use of Linear Muffin Tin Orbital (LMTO) calculations within the local spin density approximation, as implemented in the STUTTGART TB-LMTO-ASA program.[14] Starting structures for LMTO calculations were obtained from the results of volume optimization using WIEN2K. Two important tools have been used to visualize the electronic Structure of these phases. The crystal orbital Hamiltonian population (COHP) [15] enables the repartitioning of densities of states into regions which are pairwise bonding, non-bonding, and antibonding. The

8 electron compounds with $X = \text{Li}$							
XYZ	$a_{\text{Calc.}} (\text{\AA})$	$a_{\text{Exp.}} (\text{\AA})$	χ_X	χ_Y	χ_Z	Gap (eV)	B (GPa)
LiMgN	5.072	4.955	0.98	1.31	3.04	2.51	80.1
LiMgP	6.028	6.021	0.98	1.31	2.19	1.92	49.6
LiMgAs	6.218	6.19	0.98	1.31	2.18	1.55	42.9
LiMgBi	6.803	6.74	0.98	1.31	2.02	0.64	30.3
LiZnP	5.707	5.779	0.98	1.65	2.19	1.23	65.4
LiCdP	6.118	6.087	0.98	1.69	2.19	0.85	52.8
LiAlSi	5.937	5.930	0.98	1.61	1.90	0.45	62.8

Table 1. Results of density functional calculations on Li YZ phases, with experimental cell parameters for comparison. Cell parameters and bulk moduli are from LAPW calculations, and band gaps from LMTO calculations.

electron localization function (ELF)[16, 17] is a real-space indicator of the extent to which electrons are localized, and display a strong Pauli repulsion. The ELF therefore serves to locate bonding and non-bonding electron pairs in the real space of the crystal structure. A real-space bonding analysis of half-Heusler compounds has not, to our knowledge, been previously carried out.

3. Results and discussion

3.1. 8-electron compounds

We have examined 7 compounds Li YZ with the half-Heusler structure using LAPW and LMTO calculations. Results from the calculations are summarized in Table 1. The calculated cell parameters match very well with experimental cell parameters obtained from standard tabulations.[18] For LiMgN, the experimental cell parameter is from Kuriyama *et al.*[19] This suggests that in all cases, the assignment of atomic positions, which is not always a simple matter to determine from x-ray diffraction, is well justified. We discuss these results here in detail.

In the three panels of Figure 2, we compare the densities of states near the Fermi energy (taken as the top of the valence band, and set as the origin) for 6 different Li YZ half-Heusler compounds. In panel (a) of this figure two compounds LiMgN and LiMgBi are compared. Both compounds have a well defined band gap. Replacing N with the heavier pnictogens P, As, (DOS not shown) or Bi found to narrow the band gap due to the increasing band width of both the valence and conduction bands. If the X and Z ions are held constant, as in LiMgP and LiCdP, we observe that replacing the more ionic Mg by the softer Cd also results in a narrowing of the band gap. In panel (c) we compare LiAlSi with isoelectronic Si in the diamond structure. The electronic structures display a remarkable similarity in the nature and extents of the valence and conduction bands. This strong similarity has been noted previously by Christenson[20] and is fully in keeping with the description of LiAlSi being a Zintl or valence compound,[21] wherein

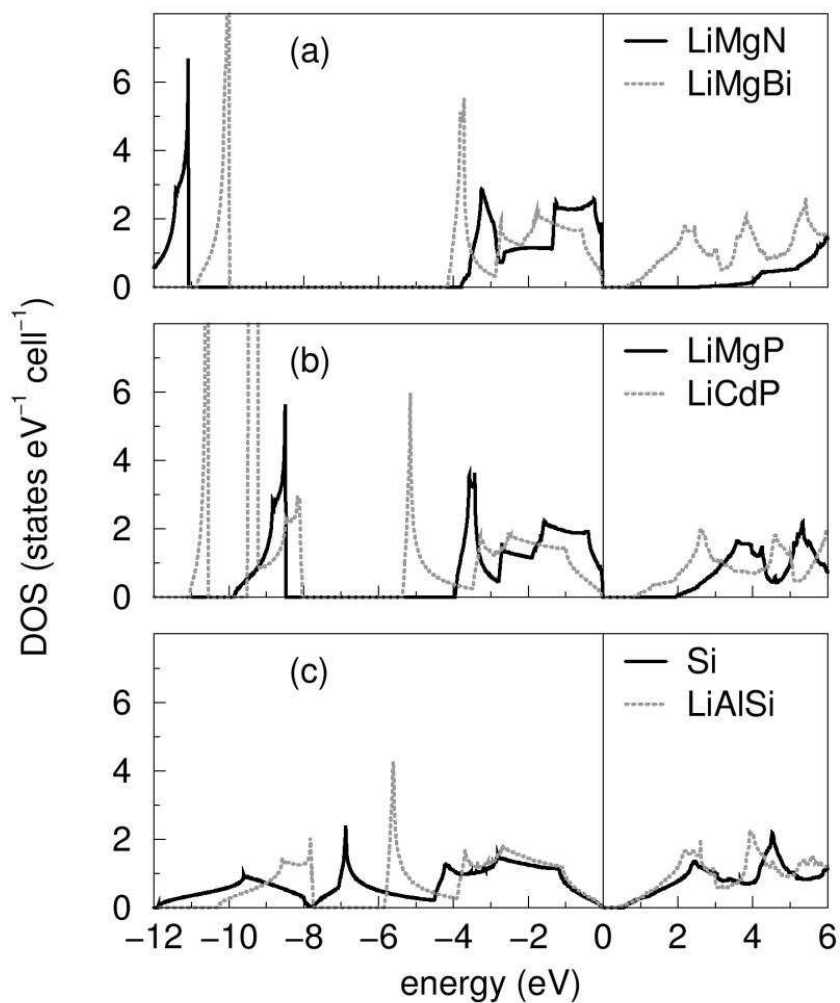


Figure 2. LMTO densities of state for a number of different Li-based half-Heusler phases compared with diamond Si.

the identical electron counts of $(\text{AlSi})^-$ and (SiSi) in turn imply that the structures would be similar. It should be noted that Mg_2Si in the fluorite structure also obeys the same rule, if we recognize it can be recast as $\text{Mg}^{2+}(\text{MgSi})^{2-}$ with the $(\text{MgSi})^{2-}$ crystallizing in a zinc blende lattice. Indeed the electronic structure of MgSi_2 [22] is quite similar to what we find for LiAlSi . The change in the space group, comparing $(Fm\bar{3}m)$ Mg_2Si and $(F\bar{4}3m)$ LiAlSi arises because the atoms in the X and Y sites in the former are identical.

The similarity in the electronic structures of Si and stuffed zinc blende compounds is further emphasized through an analysis of the Si-Si, the Al-Si, and the Mg-N COHPs of the three different compounds: Si, LiAlSi , and LiMgN , shown in Figure 3. The dashed line in this figure is an integration of the COHP up to E_F , yielding a number that is indicative of the strength of the bonding. Not only are the extents of the bonding and antibonding COHPs of Si and LiAlSi very similar, but so is the value of the integrated COHP: near -1.5 eV *per* interaction for Si and for LiAlSi . We interpret this as indicative

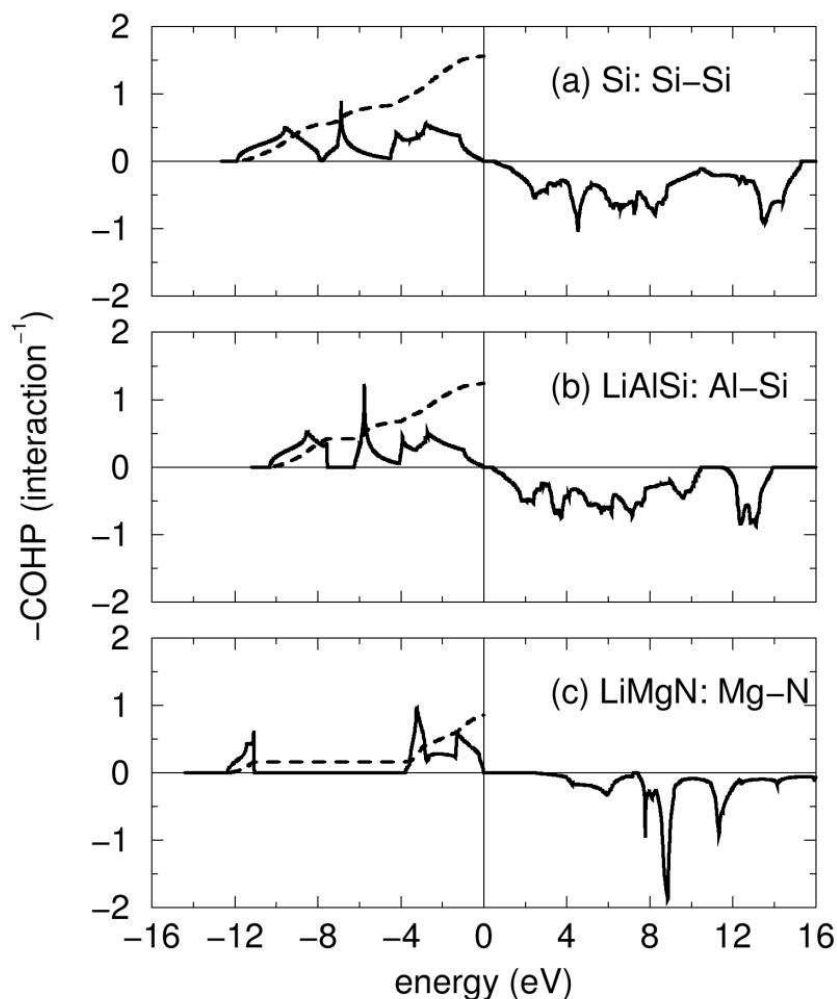


Figure 3. Crystal orbital Hamiltonian populations (COHPs) for pairwise interactions in diamond Si, LiAlSi, and LiMgN. The dashed lines are integrations of the COHPs.

of very similar extents of covalency in the diamond lattice of Si and the zinc blende sublattice of LiAlSi. This value is slightly reduced in the more polar LiMgN, and the nature of the COHP is different as well.

In Figure 4, we compare the electron localization function (ELF) for the three compounds, Si, LiAlSi, and LiMgN. Panels (a), (b), and (c) display isosurfaces of the electron localization function for values of 0.90, 0.90, and 0.825 respectively. These are high values of localization (the ELF scale as used here [17] runs from 0 through 1) and indicate highly covalent bonding between Si (cyan spheres) in the elemental structure, as well as between Al (blue) and Si (cyan) in LiAlSi, and between Mg (blue) and N (cyan) in LiMgN. The ELF takes on a curious hemispherical shape in LiMgN, reflecting the large electronegativity difference between Mg and N. The blob of localization is also closer to N than it is to Mg. It must be noted that there is no localization around Li (orange spheres) in either LiAlSi, or LiMgN, as seen also from the map of the ELF projected on the (010) plane at the rear of the unit cells. Li behaves effectively like

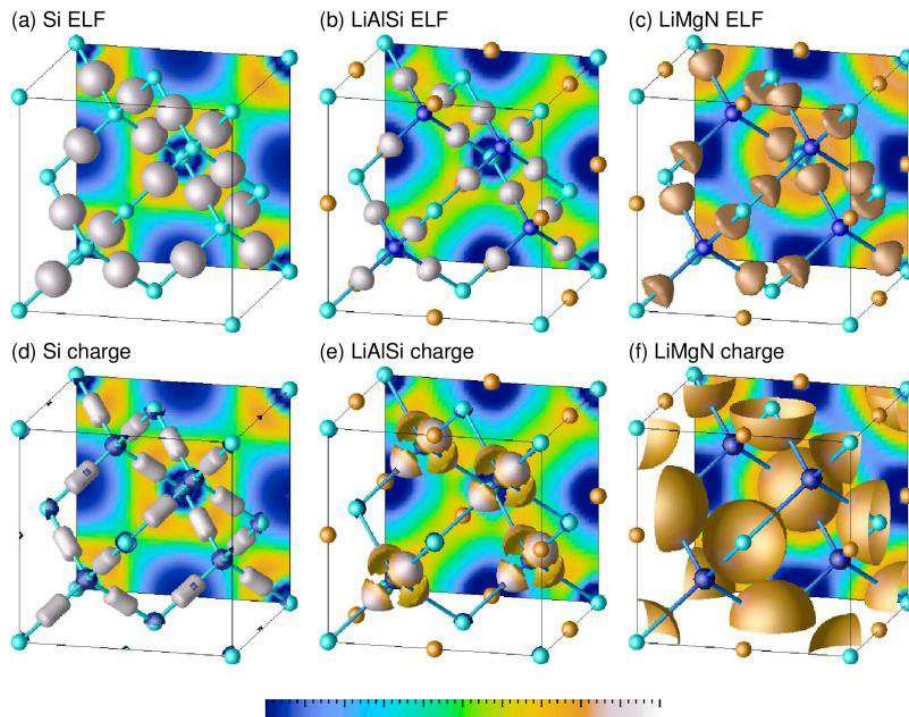


Figure 4. (Color) (a), (b), and (c) are electron localization isosurfaces for ELF values of 0.9, 0.9, and 0.825 respectively for the three compounds Si, LiAlSi, and LiMgN. (d), (e), and (f) are isosurfaces of constant charge density at a value of $0.06 e \text{ \AA}^{-3}$. The isosurfaces are decorated by the value of the electron localization function. The color-bar at the bottom of the figure indicates increasing localization from left (0.0) to right (1.0). The positions of atoms are as in Figure 1, with Z at the origin *etc.*.

ionic Li^+ . In panels (d), (e), and (f) of this figure, we display isosurfaces of charge for a value of $0.06 e \text{ \AA}^{-3}$ within the space of the unit cell. The charge isosurfaces have been decorated (colored) by the ELF. Bonds distort charges from being spherical, so distortions should be interpreted as covalency. Ionic species on the other hand, would have spherical charge around the nucleus. We observe the highly covalent nature of the diamond lattice in Si, and the zinc blende sublattice in LiAlSi. For LiMgN, while the bonding is still covalent, the charge is closer to the more electronegative nitrogen. The fact that the charge is spherical rather than directed along the bond suggests that an anionic description might be equally valid.

Having established that at least the XYZ half-Heuslers with $X = \text{Li}$ can be written $\text{Li}^+(\text{YZ})^-$, we use the data in Table 1 to examine systematics in the band gaps of these compounds. We find the computed (LMTO) gaps of LiYZ to vary approximately as the difference of the Pauling electronegativities of Y and Z . The larger the difference in electronegativity of the species in the zinc-blende sublattice (Y and Z), the greater the band gap as a result of band narrowing. The trend cannot be used quantitatively, but only as an indicator of the Phillips-van Vechten-like[23] behavior that is seen in these complex semiconductors. It should be noted that the siting of Y in the tetrahedral position simultaneously allows the more polar pair of X and Z to form a stable rock salt

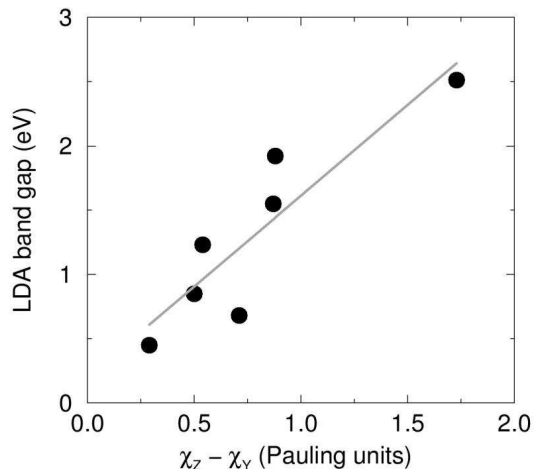


Figure 5. Dependence of the LMTO energy gap of LiYZ compounds on the difference in the Pauling electronegativities (χ) of the Y and Z species.

18 electron compounds with $X = Y$							
XYZ	$a_{\text{Calc.}}$ (Å)	$a_{\text{Exp.}}$ (Å)	χ_X	χ_Y	χ_Z	Gap (eV)	B (GPa)
YNiAs	6.104	6.171	1.22	1.91	2.18	0.53	100.0
YNiSb	6.350	6.312	1.22	1.91	2.05	0.28	92.8
YNiBi	6.475	6.411	1.22	1.91	2.02	0.13	80.9
YPdSb	6.599	6.527	1.22	2.20	2.05	0.16	92.0
YAuPb	6.842	6.729	1.22	2.54	2.33	0	70.6

Table 2. Results of density functional calculations for a number of 18-electron compounds with $X = Y$.

structure. From the viewpoint of lattice energy, this is perhaps the greater stabilizing influence on the half-Heusler structure.

3.2. 18-electron compounds

To examine whether similar rules hold for 18-electron half-Heusler compounds, we start by presenting in Table 2 the results of density functional calculations on a series of XYZ compounds where X is electropositive yttrium. The zinc blende lattice is formed by a later transition metal Y, and a main group element Z. All the compounds are semiconductors according to LMTO calculations, with band gaps ranging from 0 eV for YAuPb to 0.53 eV for YNiAs. The existence of band gaps allows us to formulate these phases according to the Zintl (or “extended Zintl”) rule $X^{3+}(YZ)^{3-}$ where $(YZ)^{3-}$ becomes isoelectronic with a diamond-structure semiconductor such as GaSb. Once again, we find a simple trend in the band gap with the difference in electronegativities of Y and Z, as seen from Figure 6.

We proceed to examine in detail, the electronic structure of select 18-electron half-Heusler compounds with different X, Y, and Z elements. Figure 7(a) displays the LMTO

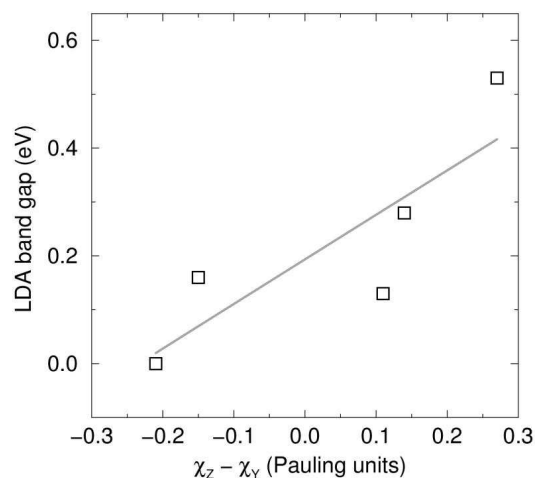


Figure 6. Dependence of the LMTO energy gap of YZ compounds on the difference in the Pauling electronegativities (χ) of the Y and Z species.

densities of state VFeSb, TiCoSb, and YNiSb, allowing the trends with changing the later transition metal Y to emerge. Projections of the densities of state on the different atomic levels (not displayed) reveal that the valence band has Y d character and Z p character. The conduction band has some of the character from these states, but in addition, has empty d states from the X atom. This fits with our expectation of the X atom being nearly fully ionized (or more accurately, having attained the group valence) and the d shell of the Y atom being filled as a result. The gap is largest for TiCoSb, and smallest for YNiSb. When both X and Y are changed, it is more difficult to seek trends in the gap. The gap in VFeSb is reduced due to V and Fe not being well separated in electronegativity. The gap in YNiSn is reduced because the unoccupied Y $4d$ states are rather broad, at least within LSDA. What is evident is that compounds with Co on the Y site have a strong propensity to maintain “clean” gaps as further seen in panel (b) of this figure where the DOS of TiCoSb, VCoSn, and NbCoSn are displayed.

From Figure 8, we see that even in these transition-metal rich phases, we can perform a bonding analysis based on COHPs. These are shown for all pairwise interactions in the two half-Heuslers VFeSb and TiCoSb. Integrating the COHPs, we find that the strongest bonding interactions are between Y and Z (Co and Sb, and Fe and Sb) while the interactions between the early and late transition metal (Ti and Co, and V and Fe) are also significant. The compounds are electronically very stable as seen from a complete absence of any antibonding interaction below the top of the valence band. The fact that the 18-electron compounds are clearly valence compounds with the band gap being located between bonding and antibonding levels supports our description of these phases being Zintl-like. The band gaps in VFeSb and TiCoSb would seem to be determined by bonding between X and Y , so at first sight, it would seem that at least these two transition-metal rich phases should not be described simply as cation-stuffed zinc blendes. However, as we shall see from the ELF analysis, the *localized* bonding remains in the zinc blende YZ lattice. Weak bonding and antibonding COHPs

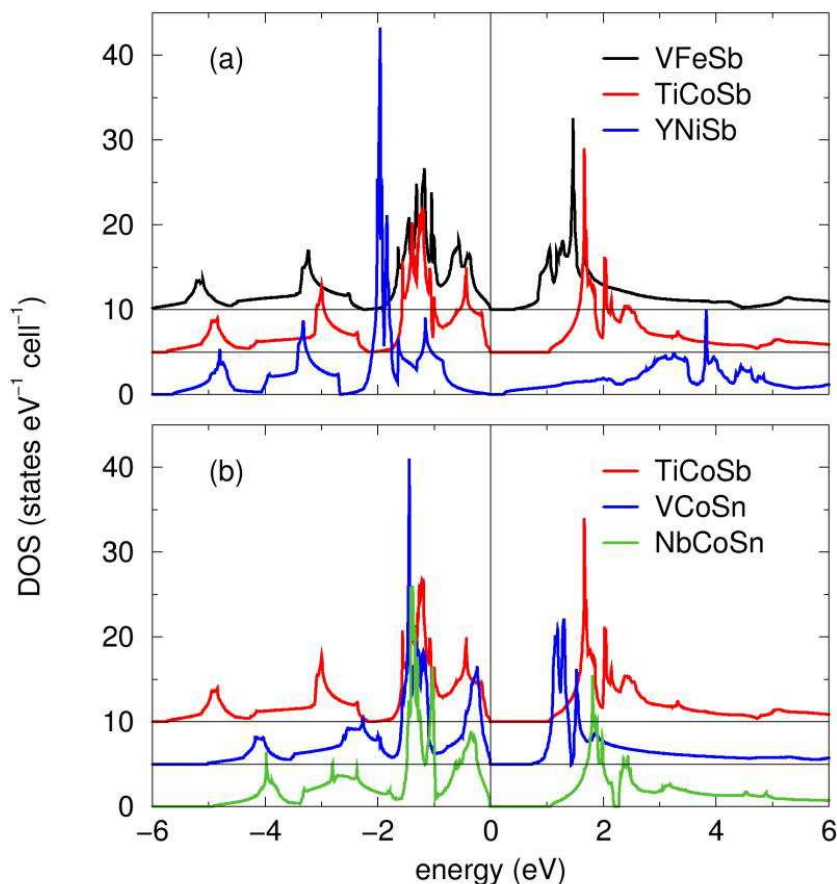


Figure 7. (Color) LMTO densities of state for the 18-electron half-Heusler compounds (a) VFeSb, TiCoSb, and YNiSb, showing how changing the nature of the Y atom affects the band gap, and for (b) TiCoSb, VCoSn, and NbCoSn emphasizing the propensity of Co-based half-Heuslers to possess a “clean” gap. The plots have been offset for clarity.

between X and Z (Ti and Sb, and V and Sb) support the view that the XZ rock salt sublattice is ionic in character.

Figure 9, displays electron localization functions for the two 18-electron half-Heusler compounds for which the COHPs are displayed in Figure 8, namely TiCoSb and VFeSb. The ELFSs, visualized respectively for values of 0.73 and 0.71 in Figure 9(a) and 9(b) are clearly indicative of strongly covalent bonding in the zinc blende sublattice, with TiCoSb displaying the greater tendency to covalent bonding. As we observed in the 8-electron compounds, localization isosurface is closer to the more electronegative Sb atoms. It must be pointed out here that the ELF is notoriously difficult to apply in d electron system, and the fact that the localization emerges so clearly here is compelling evidence for dealing with these systems as if they were valence compounds with strongly covalent bonding.

The valence charge densities displayed in Figure 9(c) and 9(d) are very distinct from what was seen for the 8-electron compounds, because the filled d shell on Y forms a large nearly spherical blobs around that atom, visualized for a charge density of $0.06 e \text{ \AA}^{-3}$.

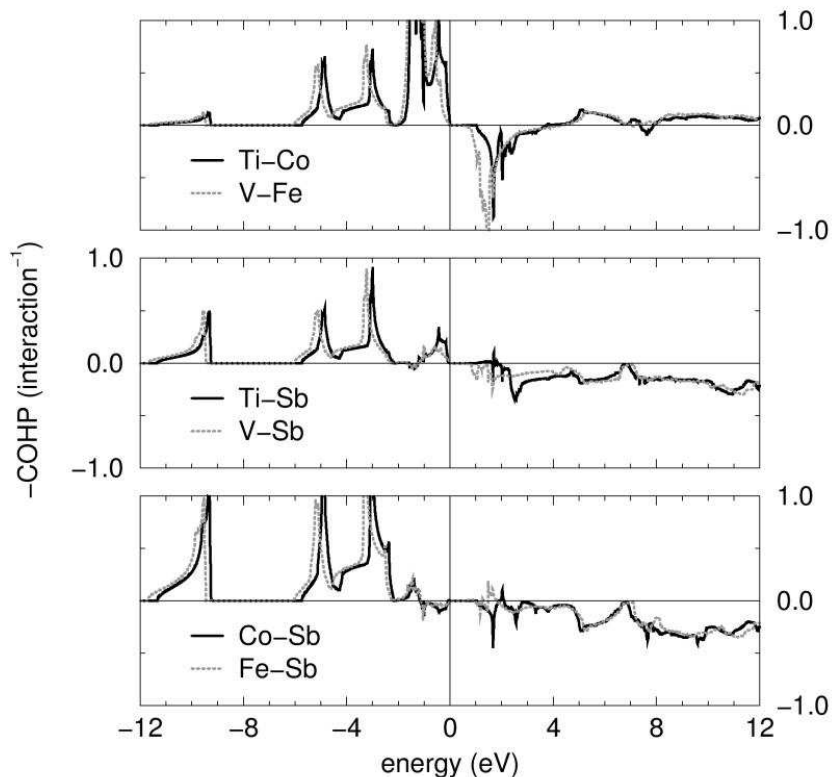


Figure 8. Crystal orbital Hamiltonian populations for all pairwise interactions in VFeSb and TiCoSb.

We find that these blobs of charge are pulled out into four strongly localized (as seen from the coloring) lobes arranged tetrahedrally and facing Z . Interestingly, in VFeSb, there is also some d -like localization around V, and there is some little localization seen on the isosurface between V and Fe. The smaller electronegativity difference between V and Fe, when compared with the electronegativity difference between Ti and Co, in conjunction with the nature of COHPs displayed in Figure 8 leads us to point this out as the origin for the smaller band gap of VFeSb. Another argument that one can proffer is that TiCoSb has greater polar intermetallic character,[24, 25, 26] with strong covalent Ti-Co bonds. V and Fe are closer together in electronegativity, and the high formal charge state (V^{5+}) is much more covalent. This results in a smaller band gap in VFeSb.

In the next subsection, we will point out that these simple ideas of covalent bonding can be carried over to the important magnetic half-Heusler compounds.

3.3. Magnetic compounds

The results of LAPW optimization of X CoSb compounds are presented in Table 3, with experimental cell parameters presented for comparison for the known compounds ($X = \text{Ti, V, and Mn}$). The table also presents the computed (LAPW) bulk modulus, which is seen to go through a maximum for TiCoSb, associated, as we will observe in the COHPs,

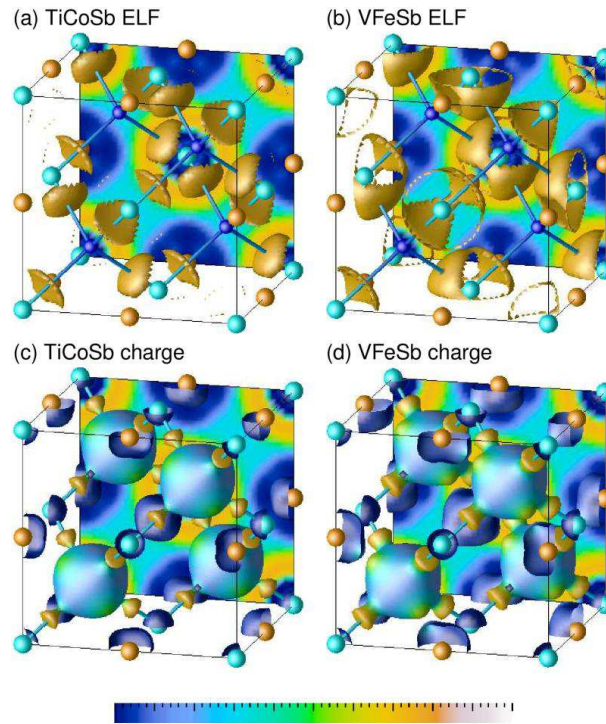


Figure 9. (Color) (a) and (b) are ELF isosurfaces for TiCoSb and VFeSb for values of 0.73 and 0.71 respectively. (c) and (d) are charge densities for a value of $0.06 e \text{ \AA}^{-3}$, decorated by the ELF.

XCoSb					
X	$a_{\text{Calc.}}$	$a_{\text{Exp.}}$	B (GPa)	n_V	M
Sc	6.095	N.A.	110.5	17	0
Ti	5.888	5.884	151.5	18	0
V	5.823	5.802	150.8	19	1
Cr	5.820	N.A.	135.4	20	2
Mn	5.810	5.875	139.1	21	3

Table 3. Optimized (LAPW) and experimental cell parameters for the the half-Heusler compounds $X\text{CoSb}$. The computed bulk moduli are also indicated. n_V is the number of valence electrons and M is the magnetic moment obtained from LMTO calculations.

with a completely filled *bonding* valence band and an empty, *antibonding* conduction band. Figure 10 displays densities of state for $X\text{CoSb}$ phases with $X = \text{Sc}, \text{Ti}, \text{V}, \text{Cr}$, and Mn. The number of valence electrons n_V per formula unit are indicated within each panel. The DOS are plotted in the two spin directions in each panel, even for the non-magnetic compounds. The compound ScCoSb is not known, and neither is CrCoSb . The non-existence of CrCoSb could be associated with the high peak in the densities of state at E_F for this compound. The (hypothetical) compound ScCoSb is not magnetic within LMTO-LSDA because the bands are too broad for the Stoner criterion to be

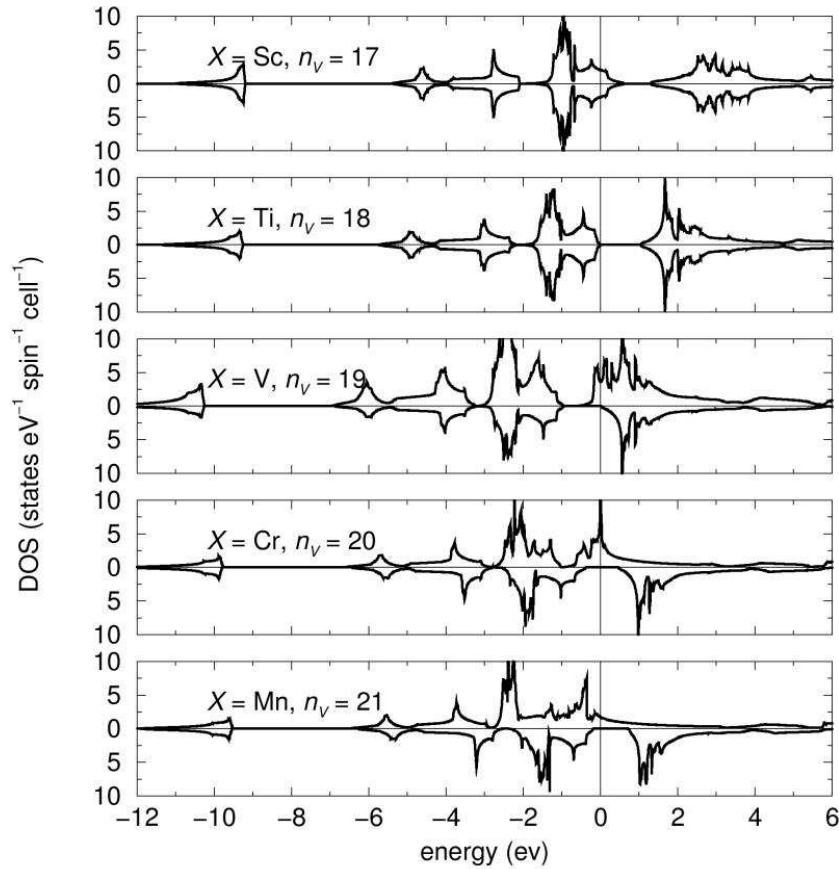


Figure 10. Densities of state of the half-Heusler compounds $X\text{CoSb}$, plotted separately in the two spin directions. The number of valence electron (n_V) in each formula unit are also indicated.

fulfilled.

All compounds except ScCoSb obey the Slater-Pauling rules for half-Heuslers, $M = n_V - 18$. TiCoSb with $n_V = 18$ is a non-magnetic semiconductor, and the calculated moments (Table 3) for VCoSb , CrCoSb , and MnCoSb are precisely 1, 2, and $3 \mu_B$. This means that these three compounds are half-metals, as seen from the densities of states in Figure 10. In particular, CrCoSb , and MnCoSb have “clean” gaps in the minority spin direction. With increasing n_V , we notice that the d states above the Fermi energy, which are derived from the electropositive X atom drop down with respect to the filled d states on Co both because of their partial filling as well as because of the well known tendency of transition metal d levels to be stabilized in energy on going across the d series.[27, 28] One of the consequences of the narrowing of the d separation between Y and X is that for larger valence electron counts than 21 or 22 (found when $Y = \text{Ni}$), half-Heuslers become unstable with respect to other structure types.

In the different panels of Figure 11, we display COHPs for X -Co, X -Sb, and Co-Sb interactions ($X = \text{V}$ or Mn). These are half-metallic ferromagnets with 19 (VCoSb) or 21 (MnCoSb) so the COHPs are spin-resolved. While the X -Sb interaction within the rock-

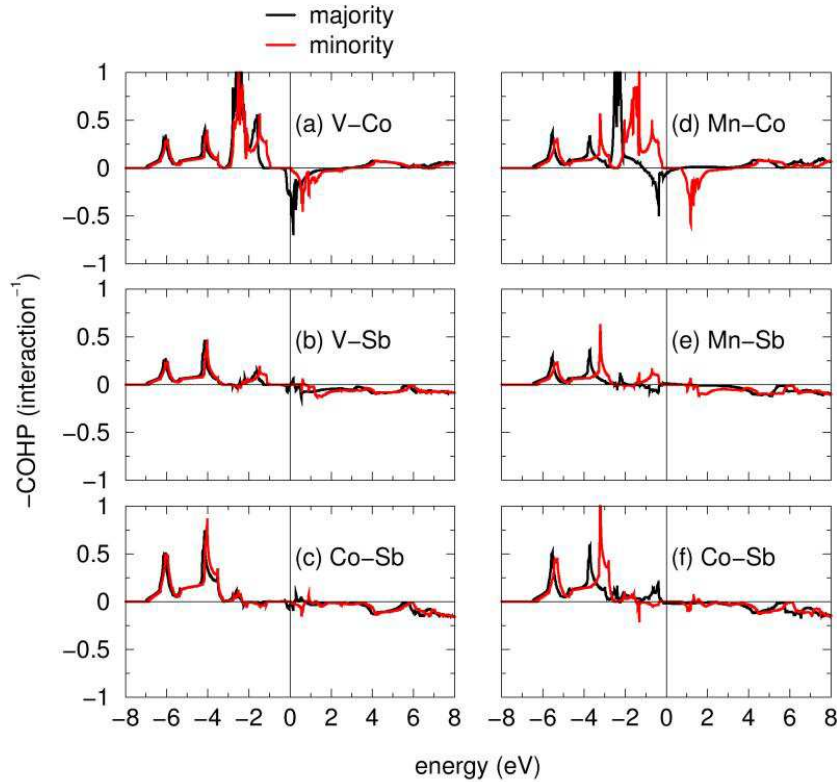


Figure 11. (Color) COHPs of VCoSb and MnCoSb in the two spin directions. In the absence of spin-orbit coupling, majority and minority spin states do not interact.

salt sublattice is clearly negligible, both X -Co and Co-Sb are seen to be important. The X -Co interaction is seen to be highly spin-polarized. The origin of the half-metallicity is revealed by the clear separation of antibonding *majority* states which cross the Fermi energy from the antibonding *minority* states which are separated by a gap equal to the exchange energy. This allows us to make the following generalization: The 18-electron half-Heuslers are the most stable phases, with well separated bonding and antibonding states. Additional electrons (more than 18) must go into antibonding states and these are split by spin-polarization and separated into majority and minority states. While these compounds are intrinsically less stable than the 18-electron compounds, they maximize their stability by ensuring that minority antibonding states remain unoccupied. The Co-Sb interaction in these two compounds is seen to be strongly covalent, but not very much affected by spin-polarization. There remains a clear separation of bonding from antibonding states as we had observed in the 18-electron semiconductors.

Real-space visualizations of the electronic structure in Figure 12 reveal that even in the magnetic compounds X CoSb with $X = V$ or Mn, the ELF's are strongly localized on the bonds of the zinc blende CoSb network. As could be anticipated from the similarities in the COHPs, there is almost no change in the Co-Sb localization pattern on going from 19-electron VCoSb to 21 electron MnCoSb [Figure 12(a) and (d)]. There

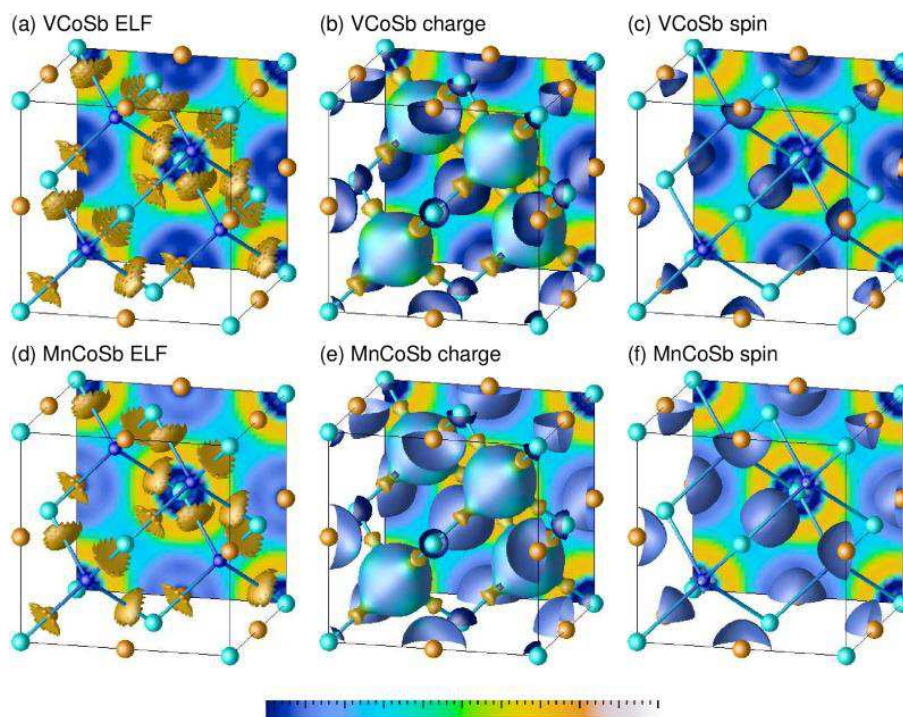


Figure 12. (Color) (a) and (d) are ELF isosurfaces for VCoSb and MnCoSb for ELF values of 0.71. (b) and (e) are charge densities for a value of $0.06 e \text{ \AA}^{-3}$, decorated by the ELF. (c) and (f) are isosurfaces of constant spin of value $0.05 \text{ spins \AA}^{-3}$.

is a strongly localized region slightly closer to the more electronegative Sb atoms in both these compounds. Again, the charge density decorated by the ELF [(b) and (e)] confirm this localization. The d electron density around Co is spherical apart from the four lobes facing Sb. What is interesting is that the magnetic moment, as visualized from an isosurface of constant spin density is clearly located on the stuffing X atom in both in VCoSb and in MnCoSb, as seen in Figure 12(c) and (f). The magnetic half-Heuslers can therefore be regarded as zinc-blende lattices of a late transition metal and a main group element, stuffed by relatively electropositive magnetic ions. Despite the presence of magnetic X^{n+} transition metal ions, the YZ^{n-} network can still be described in simple valence terms. This is reminiscent of compounds prepared by Kauzlarich and coworkers[29, 30] wherein magnetic ions such as Mn^{3+} are found to behave like electropositive cations such as Al^{3+} which donate charge to a closed shell anionic sublattice.

3.4. *MnNiSb*

For completion, we discuss in this subsection, the electronic structure of the canonical 22-electron half-Heusler compound, MnNiSb.[1] As we observed from the COHP of MnCoSb, we expect for MnNiSb that the minority gap will be formed from metal d states, and this gap will fall within the larger gap associated with the zinc blende (NiSb) sublattice. The panels of figure 13(a-d) display band structure of MnNiSb in

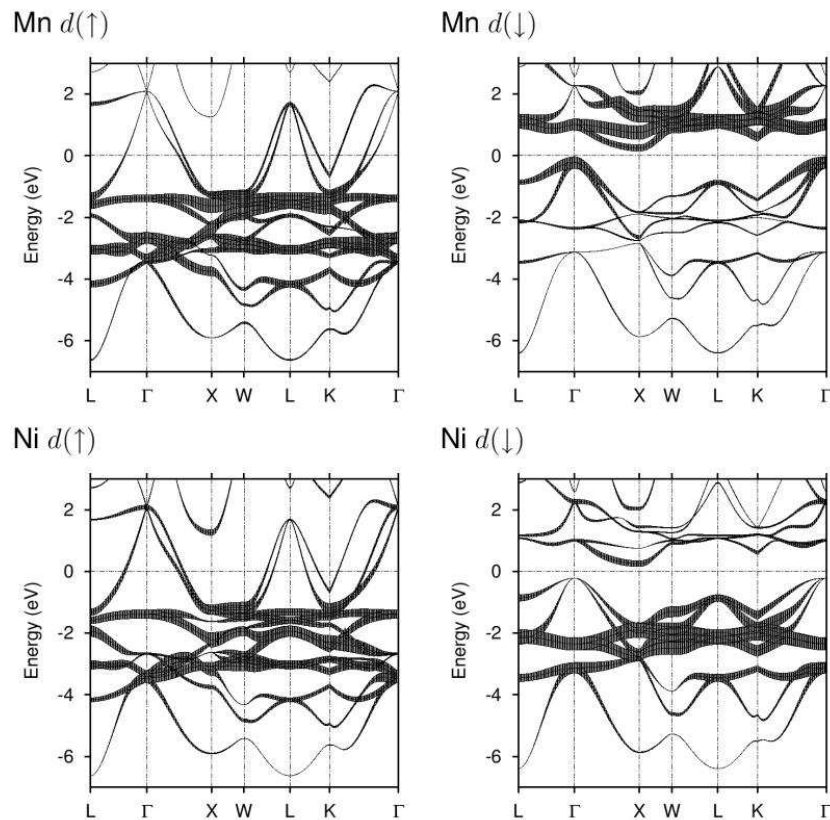


Figure 13. Band structure of MnNiSb decorated by the indicated orbital contributions from transition metal d states.

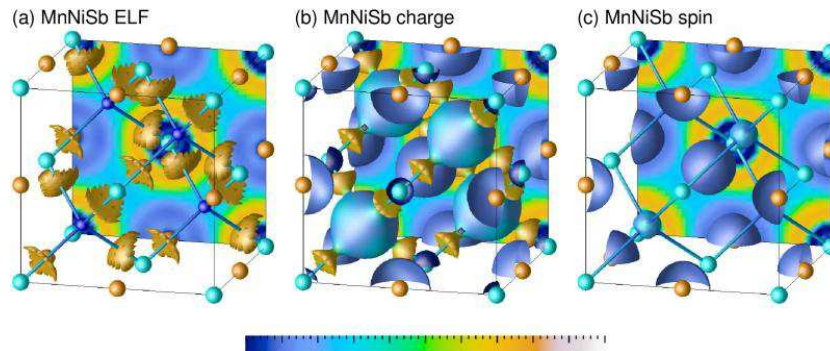


Figure 14. (Color) (a) ELF isosurfaces of MnNiSb for an ELF value of 0.73. (b) is the charge density isosurface for a value of $0.055 e \text{ \AA}^{-3}$, decorated by the ELF. (c) is an isosurfaces of constant spin density corresponding to $0.05 \text{ spins \AA}^{-3}$.

the so-called fatband representation[31] where the bands are decorated with widths proportional to various specific orbital contributions; In the different panels, the d orbitals of Mn and Ni are indicated in the different spin directions. From the band structures, it is evident that the magnetism resides largely on Mn. The valence band has Ni d character in both spin direction, but only majority Mn d states. The conduction band has minority Mn d states. The disperse majority band which traverses the Fermi

energy arises due to covalent bonding between majority Ni *d* states and majority Mn *d* states with some intermediation by Sb *p*. Indeed, we find that the disperse band going from Γ to L and Γ to X is retained even when the calculation is performed in MnNiSb where the Sb atoms are replaced by empty spheres.

Figure 14(a) and (b) display the ELF and charge of MnNiSb and confirm the picture of covalent bonding in the zinc blende network of this structure. Figure 13(c) is the spin density, and is evidently almost completely localized on Mn in this compound as suggested by the band structure.

Acknowledgments

Work at Mainz was supported by the *Deutsche Forschungsgemeinschaft* through projects FG 559 and the SPP 1166. RS gratefully acknowledges the National Science Foundation for support through a Career Award (NSF-DMR 0449354).

References

- [1] de Groot R A, Mueller F M, van Engen P G and Buschow K H J 1983 *Phys. Rev. Lett.* **50** 2024
- [2] Kübler J, Williams A R and Sommers C B 1983 *Phys. Rev. B* **28** 1745
- [3] Pierre J, Skolozdra R V, Tobola J, Kaprzyk S, Hordequin C, Kouacou M A, Karla I, Currat R and Lelièvre-Berna E 1997 *J. Alloys Compounds* **262-263** 101
- [4] Tobola J and Pierre J 2000 *J. Alloys Compounds* **296** 243
- [5] Jung D, Koo H-J and Whangbo M-H 2000 *J. Mol. Struct. Theochem* **527** 113
- [6] Stoner E C 1938 *Proc. R. Soc. Lond A* **165** 372
- [7] Galanakis I, Dederichs P H and Papanikolaou N 2002 *Phys. Rev. B* **66** 134428
- [8] Ögüt S and Rabe K M 1995 *Phys. Rev. B* **51** 10443
- [9] Wood D M, Zunger A and de Groot R 1985 *Phys. Rev. B* **31** 2570
- [10] Nowotny H and Bachmayer K 1950 *Monatsh. Chem.* **81** 488
- [11] Juza R and Hund F 1948 *Z. Anorg. Chem.* **257** 1
- [12] Nanda B R K and Dasgupta I 2003 *J. Phys. Condens. Matter* **15** 7307
- [13] Madsen G K H, Blaha P, Schwarz K, Sjöstedt E and Nördström L, 2001 *Phys. Rev. B* **64** 195134; see <http://www.wien2k.at>
- [14] Andersen O K 1975 *Phys. Rev. B* **12** 3060; Jepsen O and Andersen OK 2000 STUTTGART TB-LMTO-ASA Program version 47, MPI für Festkörperforschung, Stuttgart, Germany
- [15] Dronskowski R and Blöchl P E 1993 *J. Phys. Chem.* **97** 8617
- [16] Becke A D and Edgecombe K E 1990 *J. Chem. Phys.* **92** 5397
- [17] Silvi B and Savin A 1994 *Nature* **371** 683
- [18] Villars P and Calvert L D 1996, Pearson's Handbook of Crystallographic Data for Intermetallic Phases, 2nd Ed. ASM International, Materials Park, Ohio.
- [19] Kuriyama K, Nagasawa K and Kushida K 2002 *J. Cryst. Growth* **237** 2019
- [20] Christenson N E 1985 *Phys. Rev. B* **32** 6490
- [21] Zintl E 1939 *Angew. Chem.* **52** 1
- [22] Frøseth A G, Høier R, Derlet P M, Andersen S J and Marioara C D 2003 *Phys. Rev. B* **67** 224106
- [23] Phillips J C and van Vechten J A 1970 *Phys. Rev. B* **2** 2147
- [24] Brewer L and Wengert PR 1973 *Metall. Trans.* **4** 83
- [25] Calhorda M J and Hoffmann R 1988 *Inorg. Chem.* **27** 4679
- [26] Abdon R L and Hughbanks T 1995 *J. Am. Chem. Soc.* **117** 10035
- [27] Jobic S, Brec R and Rouxel J 1992 *J. Alloys Compounds* **178** 253

- [28] Zaanen J, Sawatzky G A and Allen J W 1985 *Phys. Rev. Lett* **55** 418
- [29] Kuramoto T Y, Kauzlarich S M and Webb D J 1992 *Chem. Mater.* **4** 435
- [30] Rehr A, Kuramoto T Y, Kauzlarich S M, Del Castillo J and Webb D J 1994 *Chem. Mater.* **6** 93
- [31] Jepsen O and Andersen O K 1995 *Z Phys B* **97** 35